AIAA 95-0466

A New High Resolution Scheme for Compressible Viscous Flow with Shocks

S. Tatsumi, L. Martinelli, and A. Jameson
Princeton University
Princeton, NJ

33rd Aerospace Sciences Meeting and Exhibit
January 9-12, 1995 / Reno, NV

A New High Resolution Scheme for Compressible Viscous Flows with Shocks

S. Tatsumi * *L. Martinelli* § and *A. Jameson* ‡
Department of Mechanical and Aerospace Engineering
Princeton University
Princeton, NJ 08544, U.S.A.

Abstract

A new flux splitting and limiting technique which yields one-point stationary shock capturing is presented. The technique is applied to the full Navier-Stokes and Reynolds Averaged Navier-Stokes equations. Calculations of laminar boundary layers at subsonic and supersonic speeds are presented together with calculations of transonic flows around airfoils. The results exhibit very good agreement with theoretical solutions and existing experimental data. It is found that the proposed scheme improves the resolution of viscous flows while maintaining excellent one-point shock capturing characteristics.

1 Introduction

Accurate and robust viscous solvers for compressible flows require the implementation of non-oscillatory discrete schemes which combine high accuracy with high resolution of shock waves and contact discontinuities. These schemes must also be formulated in such a way that they facilitate the treatment of complex geometric shapes. One of the greatest challenges of building accurate and robust Navier-Stokes solvers rests on the fact that shock capturing requires the construction of schemes which are *numerically* dissipative, a requirement which could affect the global accuracy of the solution of the *physical* viscous problem.

Recently we have analyzed a large class of schemes including High Resolution Switched schemes, Symmetric Limited Positive (SLIP) and Upstream Limited Positive (USLIP) schemes [5, 17]. SLIP and USLIP schemes were implemented and tested using several forms of flux-splitting including scalar, characteristic, and Convective Upstream Split Pressure (CUSP) schemes. Careful comparisons with analytical results for laminar boundary layers clearly indicate that the limiting process plays a greater role than the flux-splitting in determining the quality of viscous results. However, new trade-offs between the different forms of flux-splitting arise whenever crisp resolution of shocks becomes important.

Roe has shown that characteristic splitting can yield an optimal discrete shock resolution with only one interior point [15]. More recently Jameson [7, 8] has shown that a discrete shock structure with a single interior point can, in general, be supported by artificial diffusion which both:

1. produces an upwind flux if the flow is determined to be supersonic through the interface between the left and the intermediate state,
2. satisfies a generalized eigenvalue problem for the exit from the shock.

These two conditions can be satisfied by both the characteristic and CUSP schemes whereas scalar diffusion fails to satisfy the first condition.

The present work focus on the development of CUSP based schemes which combine perfect one-point shock capturing of stationary shocks with

* Visiting Research Staff, Member AIAA
§Assistant Professor, Member AIAA
‡Professor, AIAA Fellow

high resolution of boundary layers.

2 Alternative Forms of Flux Splittings

For simplicity we consider only the general one dimensional conservation law for a system of equations which can be expressed as

$$\frac{\partial w}{\partial t} + \frac{\partial}{\partial x} f(w) = 0. \tag{1}$$

Here the state and the flux vectors are

$$w = \begin{pmatrix} \rho \\ \rho u \\ \rho E \end{pmatrix}, \quad f = \begin{pmatrix} \rho u \\ \rho u^2 + p \\ \rho u H \end{pmatrix},$$

where ρ is the density, u is the velocity, E is the total energy, p is the pressure, and H is the stagnation enthalpy. If γ is the ratio of specific heats and c is the speed of sound then

$$p = (\gamma - 1)\rho\left(E - \frac{u^2}{2}\right)$$

$$c^2 = \frac{\gamma p}{\rho}$$

$$H = E + \frac{p}{\rho} = \frac{c^2}{\gamma - 1} + \frac{u^2}{2}.$$

In a steady flow H is constant. This remains true for the discrete scheme only if the numerical diffusion is constructed so that it is compatible with this condition.

It is well known that when the flow is smooth it can be represented by the quasi-linear form

$$\frac{\partial w}{\partial t} + A(w)\frac{\partial w}{\partial x} = 0,$$

where $A(w) = \frac{\partial f}{\partial w}$, and the eigenvalues u, $u + c$ and $u - c$ of the Jacobian matrix A are the wave speeds for the three characteristics. Depending on the initial data, there may not be a smooth solution of the conservation law (1). Nonlinear wave interactions along converging characteristics may lead to the formation and propagation of shock waves, while contact discontinuities may also appear.

The conservation law (1) is approximated over the interval $(0, L)$ on a mesh with an interval Δx by the semi-discrete scheme

$$\Delta x \frac{dw_j}{dt} + h_{j+\frac{1}{2}} - h_{j-\frac{1}{2}} = 0, \tag{2}$$

where w_j denotes the value of the discrete solution in cell j, and $h_{j+\frac{1}{2}}$ is the numerical flux between cells j and $j + 1$.

The numerical flux can be taken as

$$h_{j+\frac{1}{2}} = \frac{1}{2}(f_{j+1} + f_j) - d_{j+\frac{1}{2}}, \tag{3}$$

where f_j denotes the flux vector $f(w_j)$ evaluated for the state w_j, and $d_{j+\frac{1}{2}}$ is a diffusive flux which is introduced to enable the scheme to resolve discontinuities without producing oscillations in the discrete solution.

A rather general form for the diffusive flux is

$$d_{j+\frac{1}{2}} = \frac{1}{2}\alpha_{j+\frac{1}{2}} B_{j+\frac{1}{2}}(w_{j+1} - w_j),$$

where the matrix $B_{j+\frac{1}{2}}$ controls the numerical diffusion and determines the properties of the scheme, and the scaling factor $\alpha_{j+\frac{1}{2}}$ is included for convenience. Notice that since $w_{j+1} - w_j$ approximates $\Delta x \frac{\partial w}{\partial x}$, the diffusive flux introduces an error proportional to the mesh width, whence, all these schemes will be first order accurate unless compensating anti-diffusive terms are introduced.

With this notation, scalar diffusion is produced by setting

$$B_{j+\frac{1}{2}} = I, \tag{4}$$

while the characteristic upwind scheme is produced by setting

$$B_{j+\frac{1}{2}} = \left|A_{j+\frac{1}{2}}\right| = T\,|\Lambda|\,T^{-1}. \tag{5}$$

In equation (5), $A_{j+\frac{1}{2}}(w_{j+1}, w_j)$ is an estimate of the Jacobian matrix $\frac{\partial f}{\partial w}$ obtained by Roe linearization, with the property that the equation

$$f_{j+1} - f_j = A_{j+\frac{1}{2}}(w_{j+1} - w_j)$$

is satisfied exactly, and T is a similarity transformation such that

$$A_{j+\frac{1}{2}} = T\Lambda T^{-1}. \tag{6}$$

Thus, the columns of T are the eigenvectors of $A_{j+\frac{1}{2}}$, and Λ is a diagonal matrix containing its eigenvalues. The symbol $\left|A_{j+\frac{1}{2}}\right|$ is used to represent the matrix obtained by replacing the eigenvalues by their absolute values.

In this paper we are interested in an intermediate class of schemes which can be formulated by defining the first order diffusive flux as a combination of differences of the state and flux vectors

$$d_{j+\frac{1}{2}} = \frac{1}{2}\alpha^*_{j+\frac{1}{2}} c\,(w_{j+1} - w_j) + \frac{1}{2}\beta_{j+\frac{1}{2}}\,(f_{j+1} - f_j)\,. \tag{7}$$

where the factor c is included so that α^* is dimensionless. Schemes of this class are fully upwind in supersonic flow if one takes $\alpha_{j+\frac{1}{2}} = 0$ and $\beta_{j+\frac{1}{2}} = \text{sign}(M)$ when the absolute value of the local Mach number satisfies $|M| > 1$. In order to support a stationary discrete shock structure with a single interior point, α^* and β cannot be chosen independently. It turns out that once α^* is chosen, β is uniquely determined by the equilibrium at the exit of the shock, leading to a one parameter family of schemes satisfying the relation

$$\alpha^* = (1+\beta)(1-M)$$

when $M > 0$ [7]. The choice $\beta = M$ corresponds to the Harten-Lax-Van Leer (HLL) scheme [4, 2], which is extremely diffusive.

We will develop schemes of this class based on a decomposition of the flux vector f obtained by setting

$$f = uw + f_p, \tag{8}$$

where

$$f_p = \begin{pmatrix} 0 \\ p \\ up \end{pmatrix}. \tag{9}$$

Then

$$f_{j+1} - f_j = \bar{u}\,(w_{j+1} - w_j) + \bar{w}\,(u_{j+1} - u_j) + f_{p_{j+1}} - f_{p_j}, \tag{10}$$

where $\bar{u}$ and $\bar{w}$ are the arithmetic averages

$$\bar{u} = \frac{1}{2}\,(u_{j+1} + u_j)\,,\quad \bar{w} = \frac{1}{2}\,(w_{j+1} + w_j)\,.$$

This corresponds to the wave particle splitting of Rao and Deshpande [14]. Two alternative formulations of the resulting CUSP schemes are presented next.

2.1 E-CUSP formulation

Suppose that the diffusive flux is defined by equation (7). If the convective terms are separated by splitting the flux according to equations (8), (9) and (10), then the total effective coefficient of convective diffusion is

$$\alpha c = \alpha^* c + \beta \bar{u}.$$

The choice $\alpha c = \bar{u}$ leads to low diffusion near a stagnation point, and also leads to a smooth continuation of convective diffusion across the sonic line since $\alpha^* = 0$ and $\beta = 1$ when $|M| > 1$. The scheme must also be formulated so that the cases of $u > 0$ and $u < 0$ are treated symmetrically. Using the notation $M = \frac{u}{c}$, $\lambda^{\pm} = u \pm c$, this leads to the diffusion coefficients

$$\alpha = |M| \tag{11}$$

$$\beta = \begin{cases} +\max\left(0, \frac{u+\lambda^-}{u-\lambda^-}\right) & \text{if } 0 \le M \le 1 \\ -\max\left(0, \frac{u+\lambda^+}{u-\lambda^+}\right) & \text{if } -1 \le M \le 0 \\ \text{sign}(M) & \text{if } |M| \ge 1. \end{cases} \tag{12}$$

Near a stagnation point α may be modified to $\alpha = \frac{1}{2}\left(\alpha_0 + \frac{|M|^2}{\alpha_0}\right)$ if $|M|$ is smaller than a threshold α_0. The expression for β in subsonic flow can also be expressed as

$$\beta = \begin{cases} \max(0, 2M-1) & \text{if } 0 \le M \le 1 \\ \min(0, 2M+1) & \text{if } -1 \le M \le 0 \end{cases}$$

Equation (12) remains valid when the CUSP scheme is modified as described below in Section 2.2 to allow solutions with constant stagnation enthalpy. The coefficients $\alpha(M)$ and $\beta(M)$ are displayed in figure 1 for the case when $\alpha_0 = 0$. The cutoff of β when $|M| < \frac{1}{2}$, together with α approaching zero as $|M|$ approaches zero, is also appropriate for the capture of contact discontinuities.

An important property of this scheme can be illustrated by introducing a Roe linearization and by rewriting the diffusive flux as

$$d_{j+\frac{1}{2}} = \frac{1}{2}\left(\alpha^* c I + \beta A_{j+\frac{1}{2}}\right)(w_{j+1} - w_j).$$

Introducing the characteristic decomposition (6), the diffusive flux can naw be represented as

$$d_{j+\frac{1}{2}} = R\mathcal{M}R^{-1}(w_{j+1} - w_j)$$

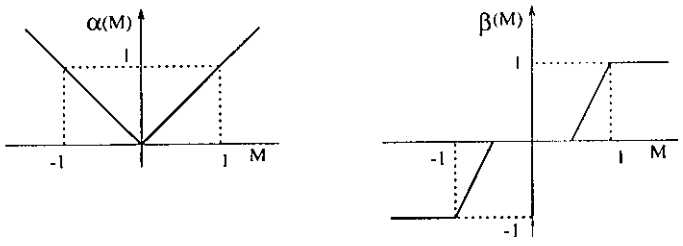

Figure 1: Diffusion Coefficients.

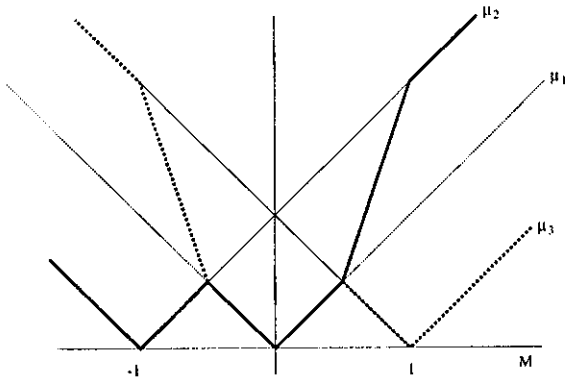

Figure 2: Eigenvalues of diffusion matrix

The matrix $\mathcal{M}$ is diagonal with eigenvalues $\mu_1 c, \mu_2 c, \mu_3 c$ given by

$$\mu_1 = \alpha - \beta M + \beta M = \alpha = |M|$$

$$\mu_2 = \begin{cases} |M| & \text{if } |M| < \frac{1}{2} \\ \alpha + \beta & \text{if } \frac{1}{2} \le M \le 1 \\ |M+1| & \text{if } |M| \ge 1 \end{cases}$$

$$\mu_3 = \begin{cases} |M| & \text{if } |M| < \frac{1}{2} \\ \alpha - \beta & \text{if } \frac{1}{2} \le M \le 1 \\ |M-1| & \text{if } |M| \ge 1 \end{cases}$$

These values are displayed in figure 2.

In the region $|M| \le \frac{1}{2}$, $\mu_1 = \mu_2 = \mu_3 = |M|$, while in the region $|M| < 1$ $\mu_2 < |M+1|$, $\mu_3 < |M-1|$. Thus the scheme has lower diffusion than the standard characteristic upwind scheme. Strict positivity is not enforced, but at a shock

$$\Delta f = A \Delta w = \mathcal{S} \Delta w$$

where $\mathcal{S}$ is the shock speed. Thus Δw must be an eigenvector corresponding to one of the eigenvalues $u \pm c$, and positivity is enforced for the corresponding characteristic variable.

2.2 H-CUSP formulation

In steady flow the stagnation enthalpy H is constant, corresponding to the fact that the energy and mass equations are consistent when the constant factor H is removed from the energy equation. Discrete and semi-discrete schemes do not necessarily satisfy this property. In the case of a semi-discrete scheme expressed in viscosity form - equations (2) and (3) - a solution with constant H is admitted if the viscosity for the energy equation reduces to the viscosity for the continuity equation with ρ replaced by ρH. Isenthalpic formulations have been considered by Veuillot and Viviand [18], and Lytton [11].

In order to extend the CUSP formulation to allow for isenthalpic solutions, we introduce the linearization

$$f_R - f_L = A_h (w_{h_R} - w_{h_L}).$$

where w_h is a modified sate vector with ρH replacing ρE. The matrix A_h may be calculated in the same way as the standard Roe linearization. In particular, by introducing the vector

$$v = \begin{pmatrix} \sqrt{\rho} \\ \sqrt{\rho} u \\ \sqrt{\rho} H \end{pmatrix},$$

all quantities in both f and w_h are products of the form $v_j v_k$ which have the property that a finite difference $\Delta(v_j v_k)$ between left and right states can be expressed as

$$\Delta(v_j v_k) = \bar{v_j} \Delta v_k + \bar{v_k} \Delta v_j$$

where $\bar{v_j}$ is the arithmetic mean $\frac{1}{2}(v_{jR} + v_{jL})$. Therefore,

$$\Delta w = B \Delta v, \;\; \Delta f = C \Delta v = C B^{-1} \Delta w,$$

where B and C can be expressed in terms of appropriate mean values of the quantities v_j. Thus, by defining

$$u = \frac{\sqrt{\rho_R}u_R + \sqrt{\rho_L}u_L}{\sqrt{\rho_R} + \sqrt{\rho_L}}, \quad H = \frac{\sqrt{\rho_R}H_R + \sqrt{\rho_L}H_L}{\sqrt{\rho_R} + \sqrt{\rho_L}},$$

and

$$c = \sqrt{(\gamma - 1)(H - \frac{u^2}{2})},$$

it follows that

$$A_h = \begin{pmatrix} 0 & 1 & 0 \\ -\frac{\gamma+1}{\gamma}\frac{u^2}{2} & \frac{\gamma+1}{\gamma}u & \frac{\gamma-1}{\gamma} \\ -uH & H & u \end{pmatrix}.$$

The eigenvalues of A_h are u, λ^+ and λ^- where

$$\lambda^{\pm} = \frac{\gamma+1}{2\gamma}u \pm \sqrt{(\frac{\gamma+1}{2\gamma}u)^2 + \frac{c^2 - u^2}{\gamma}}. \quad (13)$$

Note that λ^+ and λ^- have the same sign as $u + c$ and $u - c$, and change sign at the sonic line $u = \pm c$. The corresponding left and right eigenvectors of A_h can be computed, and are given in [7].

Using the modified linearization the CUSP scheme can be reformulated as follows to admit isenthalpic steady solutions. The diffusive flux is expressed as

$$d_{j+\frac{1}{2}} = \frac{1}{2}\alpha^* c \Delta w_h + \frac{1}{2}\beta \Delta f,$$

where Δ denotes the difference from $j+1$ to j. The split is redefined as

$$f = uw_h + f_p,$$

where

$$f_p = \begin{pmatrix} 0 \\ p \\ 0 \end{pmatrix}$$

and the diffusive flux can be expressed as

$$d_{j+\frac{1}{2}} = \frac{1}{2}\alpha c \Delta w_h + \frac{1}{2}\beta \bar{w}_h \Delta u + \frac{1}{2}\beta \Delta f_p.$$

As before, α and β are defined by equations (11) and (12), using the modified eigenvalues $\lambda^{\pm}$ defined equation (13). This splitting corresponds to the Liou-Steffen splitting [10, 19], and will be denoted as the H-CUSP scheme.

3 Implementation of limiters

In the case of a scalar conservation law, high resolution schemes which guarantee the preservation of the positivity or monotonicity of the solution can be constructed by limiting the action of higher order or anti-diffusive terms, which might otherwise cause extrema to grow. Typically, these schemes, such as both the symmetric and upstream limited positive (SLIP and USLIP) [6], compare the slope of the solution at nearby mesh intervals. The fluxes appearing in the CUSP scheme have different slopes approaching from either side of the sonic line, and use of limiters which depends on comparisons of the slopes of these fluxes can lead to a loss of smoothness in the solution at the entrance to supersonic zones in the flow. This problem can be avoided in the implementation of the CUSP scheme by forming the diffusive flux from left and right states at the cell interface. These are interpolated or extrapolated from nearby data, subject to limiters to preserve monotonicity. In a similar manner to the reconstruction of the solution in Van Leer's MUSCL scheme [9], the following construction is used.

Define the limiter

$$R(u, v) = 1 - \left| \frac{u - v}{|u| + |v|} \right|^q, \quad (14)$$

where q is a positive power which is set equal to two in the present study. Clearly $R(u, v) = 0$ when u and v have opposite sign. Also define the limited average

$$L(u, v) = \frac{1}{2}R(u, v)(u + v). \quad (15)$$

Let $w^{(k)}$ denote the kth element of the state vector w. Now define left and right states for each dependent variable separately as

$$\begin{aligned} w_L^{(k)} &= w_j^{(k)} + \frac{1}{2}L(\Delta w_{j+\frac{3}{2}}^{(k)}, \Delta w_{j-\frac{1}{2}}^{(k)}) \\ w_R^{(k)} &= w_{j+1}^{(k)} - \frac{1}{2}L(\Delta w_{j+\frac{3}{2}}^{(k)}, \Delta w_{j-\frac{1}{2}}^{(k)}), \end{aligned}$$

where

$$\Delta w_{j+\frac{1}{2}} = w_{j+1} - w_j.$$

Then

$$w_R^{(k)} - w_L^{(k)} = \Delta w_{j+\frac{1}{2}}^{(k)} - L(\Delta w_{j+\frac{3}{2}}^{(k)}, \Delta w_{j-\frac{1}{2}}^{(k)})$$

which in the case of a scalar equation reduces to the SLIP formulation [6].

For the CUSP schemes the pressures p_L and p_R for the left and right states are determined from w_L and w_R. Then the diffusive flux is calculated by substituting w_L for w_j and w_R for w_{j+1} to give

$$d_{j+\frac{1}{2}} = \frac{1}{2}\alpha^* c(w_R - w_L) + \frac{1}{2}\beta(f(w_R) - f(w_L)).$$

The alternative reconstruction:

$$\begin{aligned} w_L^{(k)} &= w_j^{(k)} + R(\Delta w_{j+\frac{3}{2}}^{(k)}, \Delta w_{j-\frac{1}{2}}^{(k)})\Delta w_{j-\frac{1}{2}}^{(k)} \\ w_R^{(k)} &= w_j^{(k)} - R(\Delta w_{j+\frac{3}{2}}^{(k)}, \Delta w_{j-\frac{1}{2}}^{(k)})\Delta w_{j+\frac{3}{2}}^{(k)} \end{aligned}$$

has been found to yield essentially identical results for calculations of steady flows.

4 Numerical Results

Extensive numerical tests have been performed with the the E and H-CUSP schemes to verify their properties [7]. Results for inviscid flow calculated with the program FLO82 verify the one-point capturing of shocks. An example of an inviscid result is presented in figure 3, where the computed pressure distribution for two grid densities is plotted together with the respective convergence histories

In this section we report the results obtained for two and three dimensional viscous flows. The two-dimensional calculations were performed with the program FLO103, which uses a cell-centered finite volume scheme to discretize the full Navier-Stokes equations. The three-dimensional calculations were performed with FLO107, which is the three dimensional extension of the original algorithm.

Time integration is carried out by a five-stage scheme which requires re-evaluation of the dissipative operators only at alternate stages [12]. This scheme couples the desirable feature of a wide stability region along both the imaginary and the real axis with good high frequency damping. The efficiency of the scheme was enhanced by using an implicit residual averaging scheme with variable coefficients, and an effective multigrid strategy which utilizes a W-cycle.

In this study it was found that 100 Multigrid Cycles were sufficient to achieve a convergence to a steady state of two dimensional viscous flows with a final level of the averaged density residuals of the order of 10^{-4}, where the initial level is the order of 1.

4.1 Flat-plate laminar boundary layer

A laminar boundary layer developing over a flat-plate at zero incidence was chosen as the first test case to validate the scheme for the viscous flow problems. The computational domain is a rectangle with the inflow boundary located two plate lengths upstream of the leading edge, and the downstream boundary located at the plate trailing edge. The upper boundary is located at a distance of four plate lengths. The mesh points are clustered in the streamwise direction near the leading edge, in order to provide adequate resolution of the flow near the stagnation point. The finest grid contains a total of 512 cells in the streamwise direction with 384 cells placed along the plate. Within the boundary layer, the grid is *equally spaced* in the boundary layer coordinate in the direction perpendicular to the plate. This ensures a constant level of resolution for all the boundary layer profiles. It also ensures that an identical resolution is achieved independently of the Reynolds number. Outside of the boundary layer the grid is exponentially stretched toward the far field. The finest grid contains a total of 128 cells in the direction normal to the plate, half of which are within the boundary layer. Three coarser grids containing respectively 8, 16, 32 cells within the boundary layer were obtained by elimination of alternate points, and they were used in the grid refinement study.

Previous studies have shown that 32 cells are generally sufficient to resolve the viscous layer [12]. Figure 4 shows the result of a grid refinement study on boundary layer velocity profiles, which was carried out to investigate the accuracy of the proposed scheme especially on coarse grids. A low value of the incoming flow Mach number ($M_\infty = .15$), well within the incompressible regime, was chosen to make a comparison with a Blasius solution meaningful. Also, this flow condition tests the numerical scheme toward its limit of applicability as $M_\infty \to 0$, and the flow becomes incompress-

ible. The Reynolds number of the incoming flow is 100,000. The results at four streamwise locations are overplotted to verify the self similarity of the computed flow. It can be seen that both of the computed tangential and transverse components of the velocity follow the self similarity law, and give an excellent agreement with the Blasius solution even on the coarsest grid with 8 cells in the boundary layer. Figure 5 shows the errors of the computed skin friction, as well as the displacement and momentum thicknesses from the Blasius solution. While the errors decrease according to the grid refinment, the values themselves are very small even in the case of the coarsest grid.

The set of calculations presented in Figure 6 is aimed at investigating the behavior of the scheme as the Mach number increases into the supersonic regime. Results are presented for a Reynolds number of 100,000, on a grid with 32 cells in the boundary layer. The supersonic result is scaled by using the Illingworth - Stewartson transformation [16], and again compared with the Blasius solution. The result shows that the scheme also accurately reproduces the boundary layer properties in the supersonic regime.

4.2 Two-dimensional turbulent flows

The first set of calculations in this section is designed to investigate the behaviour of the scheme for a turbulent flow over a two dimensional airfoil. The RAE-2822 test Case 6 was selected [3]. Two meshes were used for the computations. The first consists of a total of 512×64 mesh cells with 385 points fitted on the airfoil, while in the second one the number of cells in the normal direction has been doubled to 128. The minimum distance from the airfoil surface of the first coordinate line is 2×10^{-5} chords which corresponds to a value of $y^+ < 5$ for the assigned Reynolds number. Transition was fixed at the experimental location of the trip wire. Also the outer boundary was placed at a distance of 18 chords. A Baldwin and Lomax turbulence model [1] has been used for this grid refinement study because the flow field was expected to be attached, and the behaviour of the solution predicted by this model is reasonably well understood.

Figure 7 shows a comparison of the computed pressure coefficient along the airfoil for the two grid densities. The experimental results are also plotted as a reference. It can be seen that the computed pressure distribution is well converged on the 512×64 grid. The computed skin friction coefficient, normalized by the free stream dynamic pressure, is also is plotted in figure 7, and shows that grid independent results are obtained on the 512×64 mesh.

The next test case consists of a RC(4)-10 airfoil with a freestream Mach number of 0.59, and a Reynolds number of 7.5 million. The airfoil was designed for application to the inboard region of a helicopter main rotor blade [13]. This case was chosen to investigate further the applicability of the scheme to solve practical transonic turbulent flow problems. The turbulence model used here is again a simple algebraic Baldwin and Lomax. A C-type mesh consisting of a total of 512×64 mesh cells was used in the computations. The normal mesh spacing at the wall is 0.00002 chords, resulting in cells with aspect ratios of the order of 250:1 along the airfoil.

Figure 8 shows a comparison of the surface pressure distribution between the computed result and the experimental data at angle of attack of 3.41 degrees. The agreement is very good, including the shock location where the critical pressure coefficient for this particular Mach number is -1.36. The computed lift, drag, and pitching moment coefficients in terms of the angle of attack are shown in Figure 8 in comparison with experimental data. The agreement is again fairly good except at the higher angle of attack where steadiness of the flow is questionable.

4.3 Three-Dimensional Computations

The next test case consists of a 747-200 Wing-Body configuration. The geometry, the grid generator, and the test conditions were kindly provided by J. Yu of the Boeing Commercial Airplane Company. A calculation was run by using a relatively coarse C-H grid made up of $192 \times 64 \times 48$ cells. The free stream Mach number was set to $M = .855$, the wing was set at an angle of attack of 2.7^o. Since the flow is expected to be attached, a Baldwin and Lomax

turbulence model was used. The pressure distribution computed with the H-CUSP scheme is shown in figure 9. It can be noticed that the scheme produces a very crisp resolution of the shock structure on the top surface of the wing. The improvement over the standard scalar diffusion can be appreciated by comparing the computed pressure distributions at the wing mid-span 10. An identical grid was used for the two calculations. Again the H-CUSP scheme proved to yield superior results.

5 Concluding Remarks

A new flux splitting and limiting scheme has been developed and applied to the solution of the compressible Navier-Stokes equations. The calculations performed so far indicate that the scheme, which was originally tailored for non-oscillatory shock capturing, yields accurate solutions for viscous flows. It leads to an improvement of the overall computational efficiency by allowing the use of coarser grids. Preliminary three-dimensional viscous calculations seems to confirm this fact.

Acknowledgment

The first author gratefully acknowledges Mitsubishi Heavy Industries, Ltd. whose support has made his stay at Princeton University possible.

This work has benefited from the generous support of ARPA under Grant No. N00014-92-J-1796, and AFOSR under Grant No. AFOSR-91-0391.

References

[1] B. Baldwin and H. Lomax. Thin layer approximation and algebraic model for separated turbulent flow. AIAA Paper 78-257, 1978.

[2] B. Einfeldt. On Godunov-type methods for gas dynamics. *SIAM J. Num. Anal.*, 25:294–318, 1988.

[3] Cook P. H., Mc Donald M. A., , and Firmin M. C. P. Aerofoil rae 2822 pressure distributions , boundary layer and wake measurements. AGARD Advisory Report 138, AGARD, 1979.

[4] A. Harten, P.D. Lax, and B. Van Leer. On upstream differencing and Godunov-type schemes for hyperbolic conservation laws. *SIAM Review*, 25:35–61, 1983.

[5] A. Jameson. Computational algorithms for aerodynamic analysis and design. *Appl. Num. Math.*, 13:383–422, 1993.

[6] A. Jameson. Analysis and design of numerical schemes for gas dynamics 1, artificial diffusion, upwind biasing, limiters and their effect on multigrid convergence. *Int. J. of Comp. Fluid Dyn.*, To Appear.

[7] A. Jameson. Analysis and design of numerical schemes for gas dynamics 2, artificial diffusion and discrete shock structure. *Int. J. of Comp. Fluid Dyn.*, To Appear.

[8] A. Jameson. Positive schemes and shock modelling for compressible flows. *Int. J. of Num. Methods in Eng.*, To Appear.

[9] B. Van Leer. Towards the ultimate conservative difference scheme. V a second order sequel to Godunov's method. *J. Comp. Phys.*, 32:101–136, 1979.

[10] M-S. Liou and C.J. Steffen. A new flux splitting scheme. *J. Comp. Phys.*, 107:23–39, 1993.

[11] C. C. Lytton. Solution of the Euler equations for transonic flow over a lifting aerofoil – the Bernoulli formulation (Roe/Lytton method). *J. Comp. Phys.*, 73:395–431, 1987.

[12] L. Martinelli and A. Jameson. Validation of a Multigrid Method for the Reynolds Averaged Equations. *AIAA paper 88-0414*, January 1988.

[13] K.W. Noonan. Aerodynamic characteristics of two rotorcraft airfoils designed for application to the inboard region of a main rotor blade. NASA-TP 3009, 1990.

[14] S. V. Rao and S. M. Deshpande. A class of efficient kinetic upwind methods for compressible flows. *Report 91 FM 11*, Indian Institute of Science, 1991.

[15] P.L. Roe. Fluctuations and signals - a framework for numerical evolution prolems. In K.W. Morton and M.J. Baines, editors, *Proceedings of IMA Conference on Numerical Methods in Fluid Dynamics*, pages 219–257, Reading, 1981.

[16] H. Schlichting. *Boundary Layer Theory.* McGraw-Hill, New York, 1979. VII-th edition.

[17] S. Tatsumi, L. Martinelli, and A. Jameson. Design, Implementation, and Validation of Flux Limited Schemes for the Solution of the Compressible Navier-Stokes Equations. *AIAA paper 94-0647*, January 1994.

[18] J. P. Veuillot and H. Viviand. Computation of steady inviscid transonic flows using pseudo-unsteady methods. In A. Rizzi and H. Viviand, editors, *Notes on Numerical Fluid Mechanics, Vol. 3*, pages 45–57. Viewveg, 1981.

[19] Y. Wada and M-S. Liou. A flux splitting scheme with high-resolution and robustness for discontinuities. *AIAA paper 94-0083*, AIAA 32nd Aerospace Sciences Meeting, Reno, Nevada, January 1994.

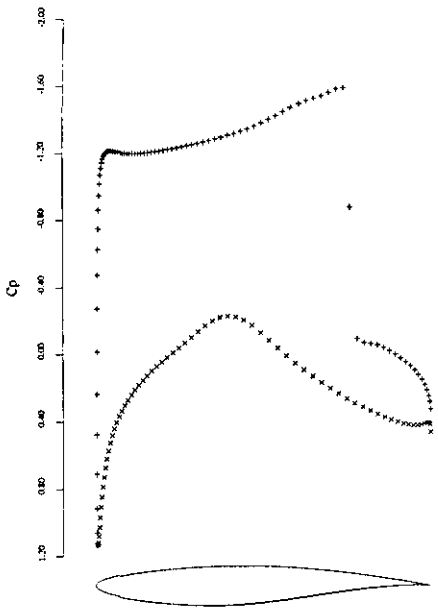

3a: C_p Distribution – Euler Equations
Rae2822 Airfoil 160×32 grid.
$M = 0.75$, $\alpha = 3^o$

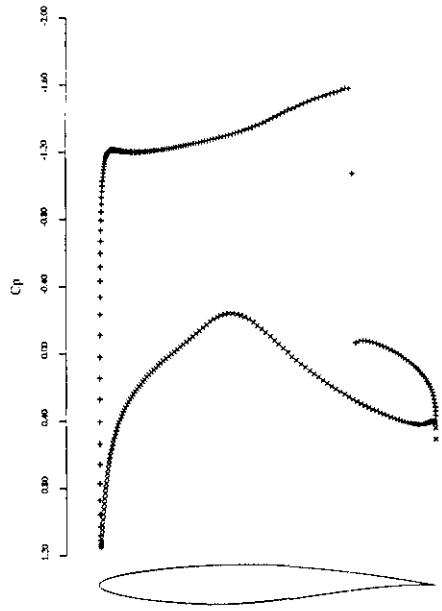

3b: C_p Distribution – Euler Equations
Rae2822 Airfoil 320×64 grid
$M = 0.75$, $\alpha = 3^o$

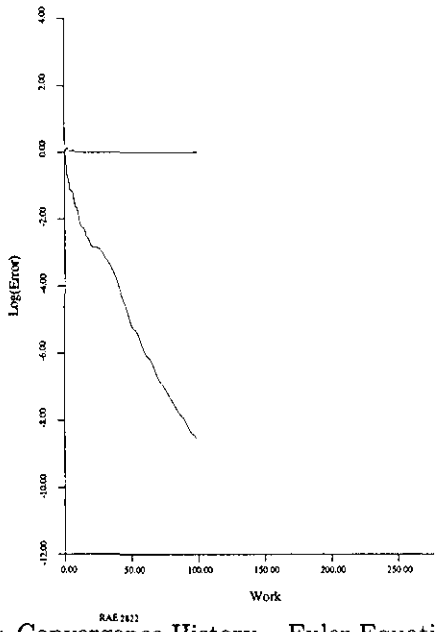

3c: Convergence History – Euler Equations
Rae2822 Airfoil 160×32 grid

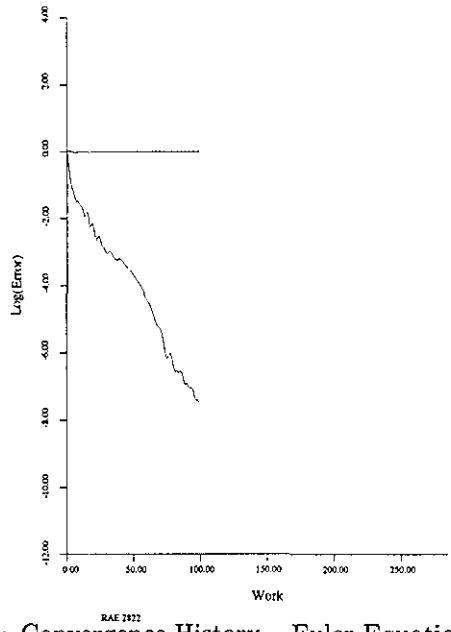

3d: Convergence History – Euler Equations
Rae2822 Airfoil 320×64 grid

Figure 3:

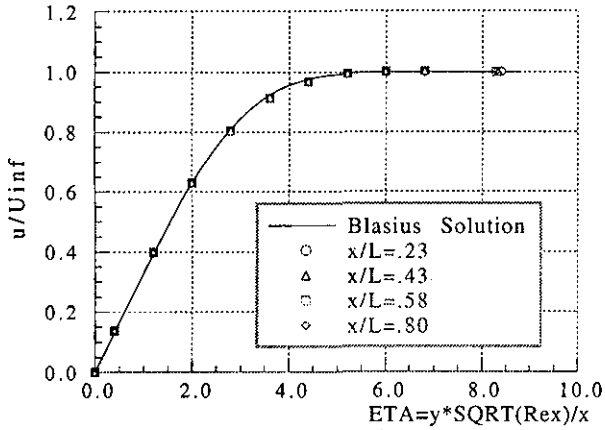

4a: Tangential velocity
8 cells in the layer

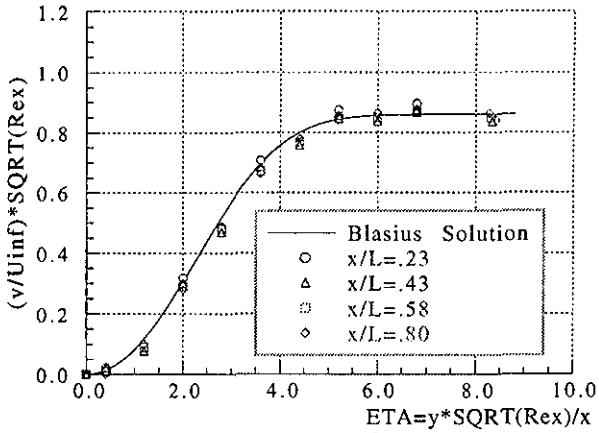

4b: Transverse velocity
8 cells in the layer

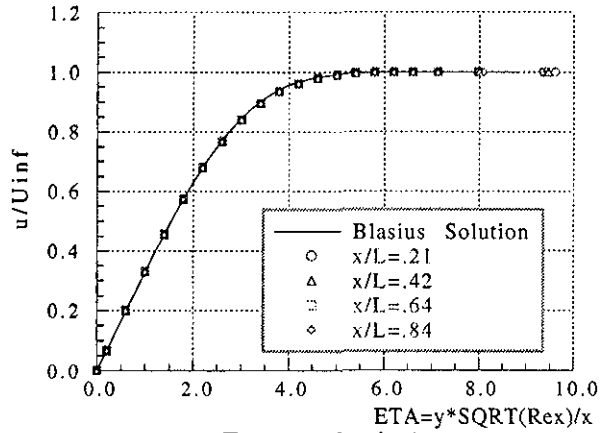

4c: Tangential velocity
16 cells in the layer

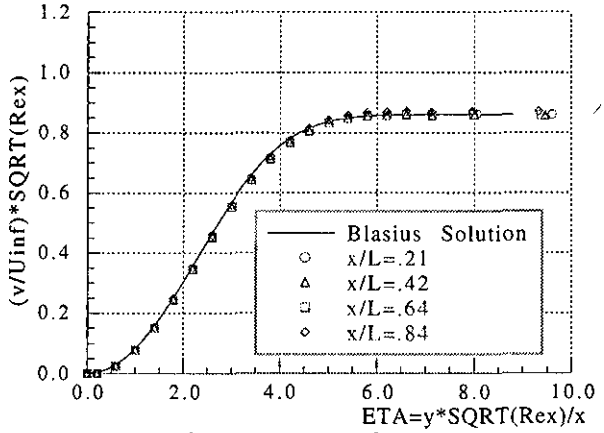

4d: Transverse velocity
16 cells in the layer

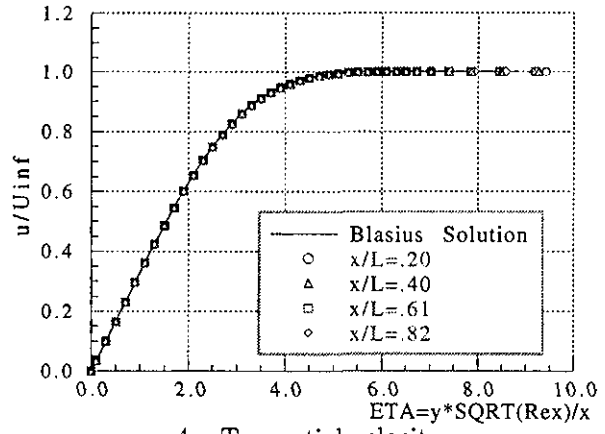

4e: Tangential velocity
32 cells in the layer

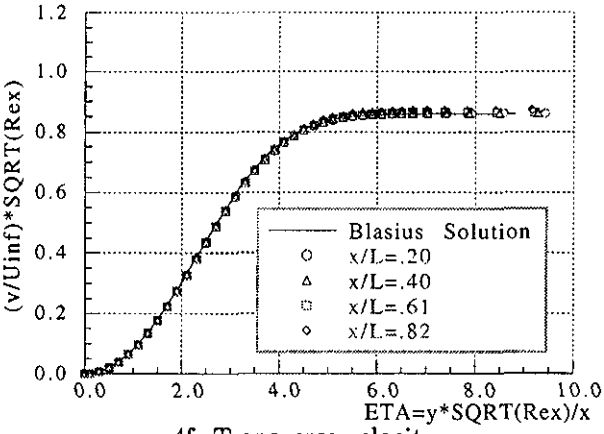

4f: Transverse velocity
32 cells in the layer

Figure 4: Boundary layer velocity profiles at $M = .15$ and $Re = 100,000$

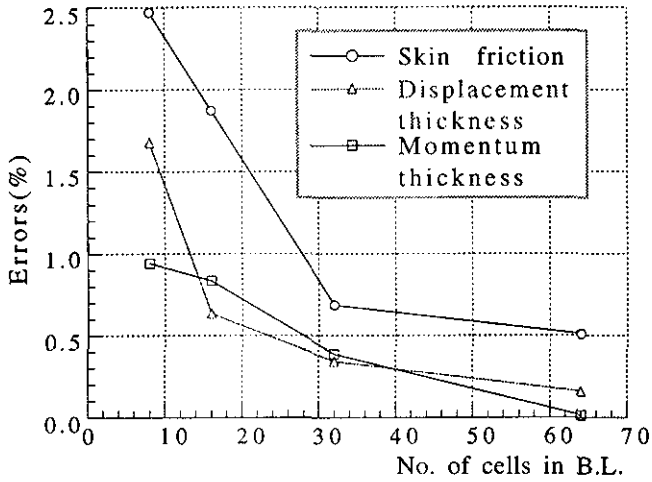

Figure 5: Comparison of computed results with the Blasius solution at $M = .15$ and $Re = 100,000$

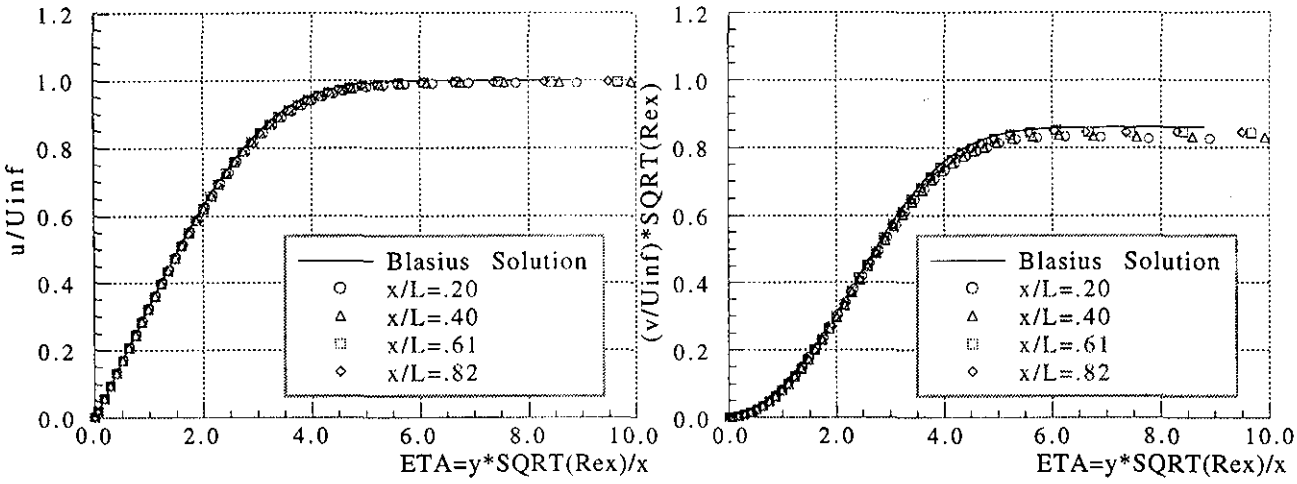

Figure 6: Boundary layer velocity profiles at $M = 2.0$ and $Re = 100,000$

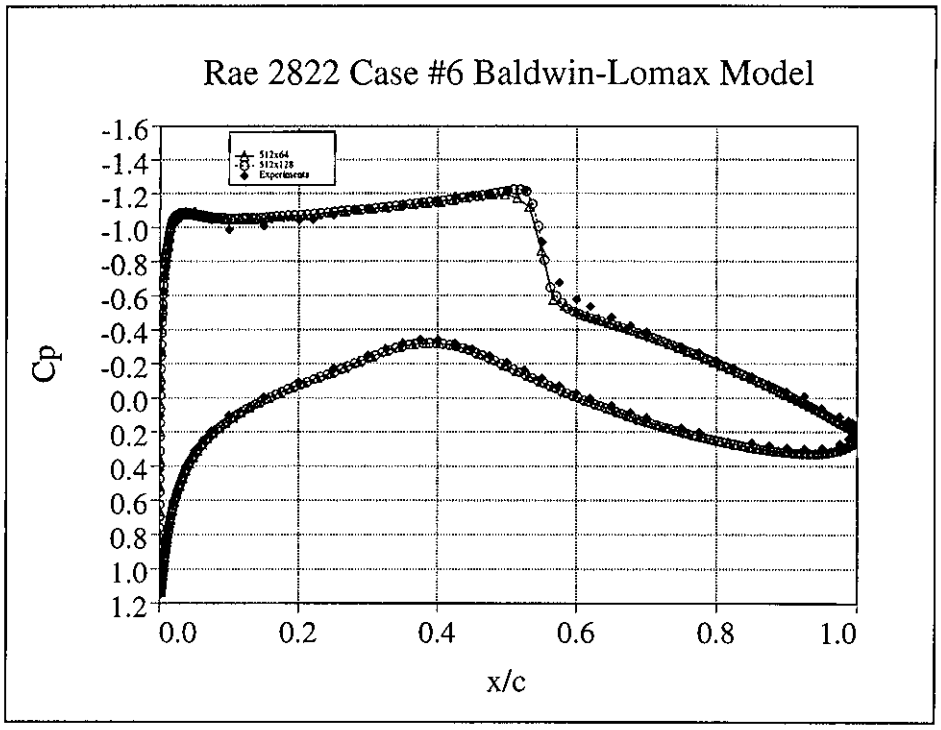

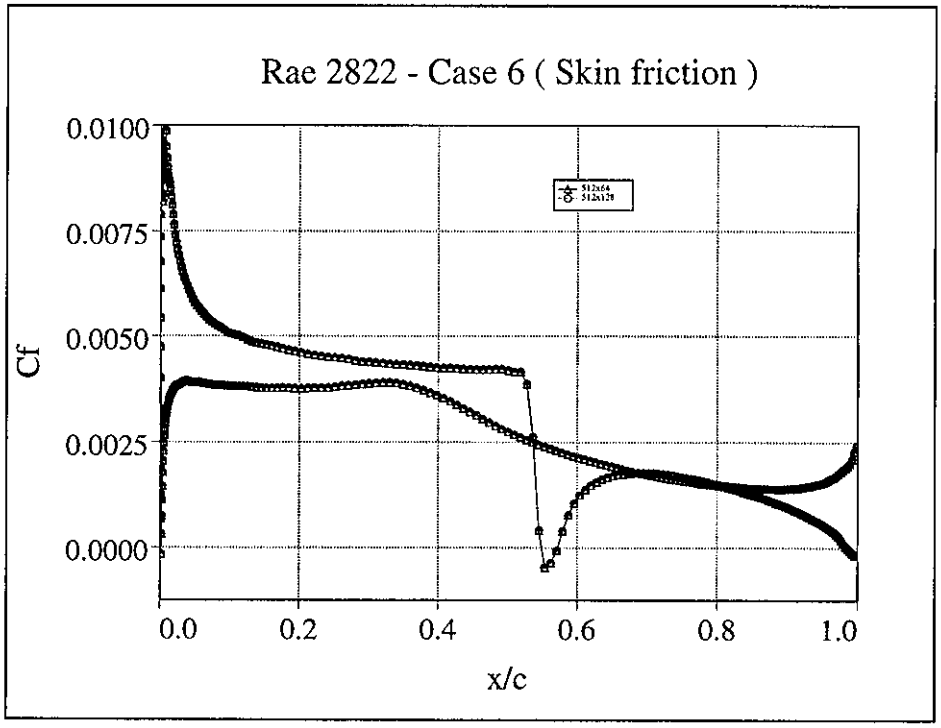

Figure 7: Rae 2822 Case 6, $M = .731$, $\alpha = 2.51^{o}$, and $Re = 6,500,000$

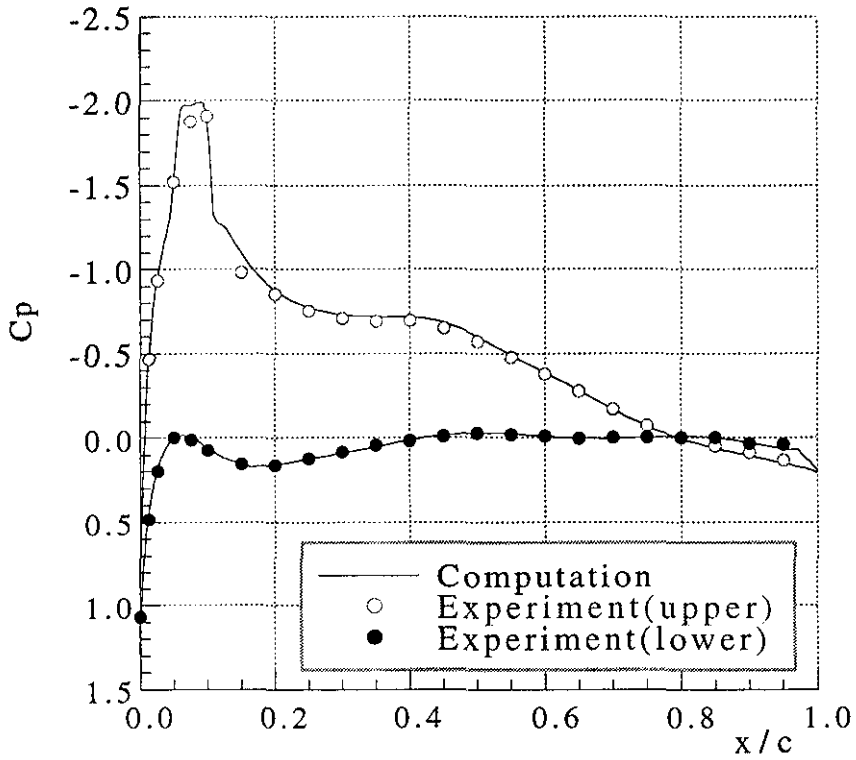

8a: Pressure distribution
$M = .59$, $\alpha = 3.41°$, $Re = 7,500,000$

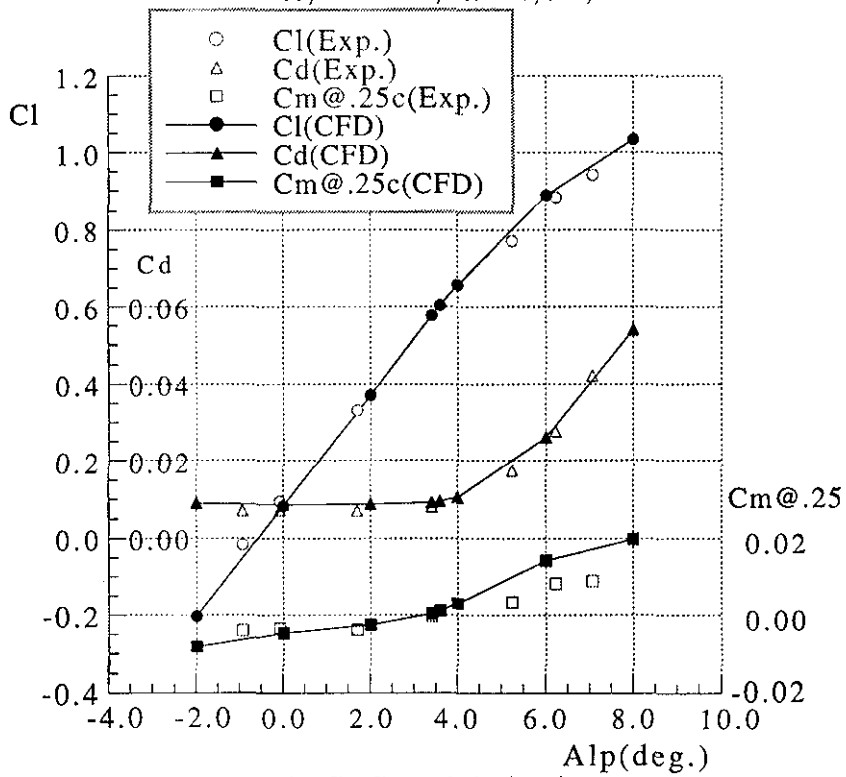

8b: C_l, C_d, and $C_m(.25c)$
$M = .59$, $Re = 7,500,000$

Figure 8: Comparison with Experimental data for RC(4)-10 Airfoil

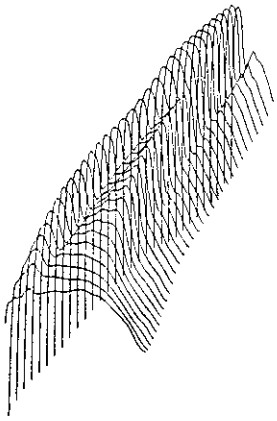

9a: Boeing-747 Wing
Pressure coefficient on the top surface

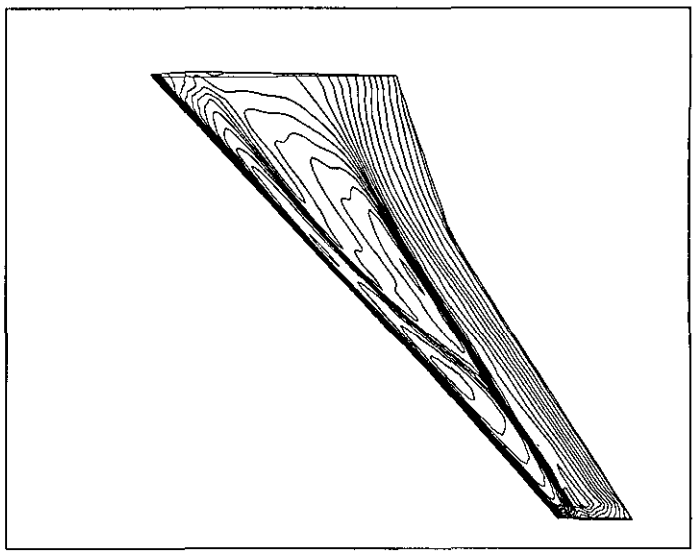

9b: Boeing-747 Wing
Pressure coefficient on the top surface

Figure 9:

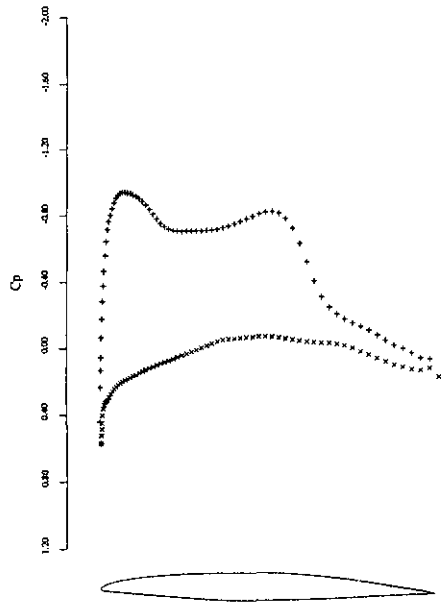

10a: C_p Distribution – Scalar Dissipation
747-200 Wing Section at 46% Span

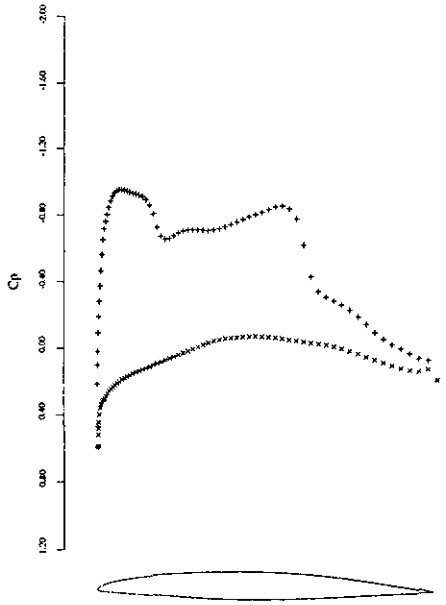

10b: C_p Distribution – H-CUSP SCHEME
747-200 Wing Section at 46% Span

Figure 10: